energies

MDPI

Article

Assessment of Dependency of Unsteady Onset Flow and Resultant Tidal Turbine Fatigue Loads on Measurement Position at a Tidal Site

Hannah Mullings *,† and Tim Stallard †

School of Engineering, The University of Manchester, Manchester M13 9PL, UK; tim.stallard@manchester.ac.uk
* Correspondence: hannah.mullings@manchester.ac.uk
† These authors contributed equally to this work.

Abstract: This work determines the variation in the fatigue loading on a tidal turbine at two depth positions and two different locations within a site. Site data were obtained at the European Marine Energy Centre, EMEC, test facility in Scotland, which has been compiled at the University of Edinburgh. The turbine modelled is the 18m Diameter DEEP-gen 1MW horizontal axis turbine. A blade element method is combined with a synthetic turbulence inflow to determine forces along the blade over a period of five tidal cycles. The focus is on establishing the difference between the loads at one tidal site, with an emphasis on the variety of turbulent conditions, with the onset flow fluctuations as great as 17% and the average integral lengthscales varying from 11 to 14 m at hub height. Fatigue loading is assessed using damage equivalent loads, with a 30% variation between turbine positions and 32% between turbine locations within a site, for one design case. When long term loading is assessed, a 41% difference is found for aggregated loads for a near surface turbine and a 28% difference for a near bed turbine.

Keywords: tidal turbine; fatigue loading; turbulence

Citation: Mullings, H.; Stallard, T. Assessment of Dependency of Unsteady Onset Flow and Resultant Tidal Turbine Fatigue Loads on Measurement Position at a Tidal Site. *Energies* **2021**, *14*, 5470. https://doi.org/10.3390/en14175470

Academic Editors: Eric L. Bibeau and Guillou Sylvain

Received: 5 July 2021
Accepted: 25 August 2021
Published: 2 September 2021

1. Introduction

To progress the development of full-scale tidal sites, there is a need to understand the loading which a turbine experiences. This loading is dependent upon the different environmental conditions at the site, conditions such as waves, shear and turbulence. These conditions are commonly measured using devices such as, Acoustic Doppler Current Profiler (ADCP), Acoustic Doppler Velocimeter (ADV) and Wave Buoys. With shear and turbulence characteristics being predicted through measurements of the ambient flow velocity, waves are usually characterised using pressure and surface profiles. Acquiring site data is a costly exercise therefore site surveys usually rely upon one device such as an ADCP collecting multiple sets of data to establish both waves and current data. Depending on the set up of the device this varies in difficulty. ADCPs measure the water velocity through each beam of the device; in most cases at least four beams are used, with an optional fifth beam vertically upwards.

This study examines the difference in loading on a turbine at two different locations within a tidal site as well as at two different depth positions. Loading on a tidal turbine can be determined using different methods, computationally and experimentally. Computationally there are two methods that can be used to calculate loading, one method is to use blade-element momentum (BEM) theory which is a numerical method utilising actuator disk theory. This approach has been validated as a useful tool to help predict performance of tidal turbines and serves as the backbone to commercial software Tidal Bladed. The other method that can be used is computational fluid dynamics (CFD) which enables the calculation of loads through the creation of actuator disk [1], actuator line [2] and fully-blade resolved models [3]. These models increase in complexity and computational cost, especially when considering an array formation of turbines and loading over

multiple conditions. This work will utilise an efficient blade element method with unsteady conditions, which has been validated against experimental work [4].

Fatigue loading is defined by the use of damage equivalent loads (DELs), these loads have been used to examine different environmental conditions by [5–7]. This method is used in the design standards to calculate fatigue [8]. In literature these loads are determined using Tidal Bladed [5,6], with [7] also using this software but including a comparison to loads on a full scale device. In order to calculate these damage equivalent loads the number of cycles and amplitude of the cycles are required. Due to the unsteady nature of the loading, the best method to determine the load cycles is the Rainflow Cycle Counting method [9]. This method enables the determination of cycles for variable amplitude loading. It examines the tensile and compressive peaks within the time history of loading and calculates the ranges between successive tensile or compressive peaks depending on whether the following peak is less than or greater than the previous peak. These ranges are considered as 'half' cycles and are summed to determine the total number of cycles. This method has been applied to determine fatigue loads for offshore components in [7,10].

The DELs are derived from a time history of loads using linear damage hypothesis to determine a single magnitude load repeating at a single frequency which would cause the same damage.

$$L_m = \left(\frac{\sum_i n_i L_i^m}{fT} \right)^{1/m}, \tag{1}$$

where n_i is the number of cycles at each binned load magnitude, m is the material gradient, f is the repetition frequency, T is the time sample length, L_i is the load bin and L_m is the damage equivalent load for specific material gradient. In order to determine the load cycles and magnitude to calculate the DELs, the time varying load is required. In this work, the axial force on a blade is used to calculate the root bending moment; The method employed here extracts the onset flow at N positions along a blade length, which rotate with time, depending on the chosen operating point. The axial (F_a) and tangential (F_t) forces along each blade are calculated using Equations (2) and (3):

$$\delta F_a(t) = \delta L(t) cos(\phi(t)) + \delta D(t) sin(\phi(t)), \tag{2}$$

$$\delta F_t(t) = \delta L(t) sin(\phi(t)) - \delta D(t) cos(\phi(t)). \tag{3}$$

The main interest here is the axial force (F_a) on each segment of the blade as this leads to the calculation of root bending moment as well as rotor thrust. Both of these results can be used to establish the respective load spectra and hence determine the load cycles enabling the fatigue loads to be predicted. In order to calculate the axial and tangential forces, the lift and drag forces are needed which are calculated using Equations (4) and (5):

$$\delta L(t) = \frac{1}{2} B \rho c (U_{rel})^2 C_L \delta r, \tag{4}$$

$$\delta D(t) = \frac{1}{2} B \rho c (U_{rel})^2 C_D \delta r, \tag{5}$$

where c is the chord length, δr is the radial width of the blade segment, B is the number of blades, ρ is the fluid density, C_L and C_D correspond to the lift and drag coefficients respectively and U_{rel} is the relative velocity determined from the onset flow, defined by Equation (6). The onset flow is also defined by the inflow angle to the blade given by $\phi(t)$, given by Equation (7):

$$\delta U_{rel}(t) = \sqrt{U_X(t)^2 + (\Omega r - U_\Theta(t))^2)}, \tag{6}$$

$$\delta \phi(t) = sin^{-1} \frac{U_X(t)}{U_{rel}(t)}, \tag{7}$$

where U_{rel} is the relative velocity to the blade which incorporates the longitudinal velocity, U_X and the components in the tangential direction, U_Θ with the angular velocity ω at each radius r.

In order to model the onset flow on the blade, the operational conditions should be known, across the swept area of the rotor, however typically this information is limited by the available measurement points. In this work, the focus is on understanding the variation of load within a design point which is considered the same, based upon the current standards. Key conditions that vary with operational point and site location are mainly related to the turbulence characteristics, any shear profiles and the wave conditions. Experimental work by [11] showed how the instantaneous loading is affected by turbulent features, which influences the power produced. The basis of the method used here relies upon a von Karman spectral turbulence model where auto-spectral density functions are used to describe real atmospheric turbulence. A three dimensional grid is synthesised to create a time series which is propagated using Taylor's frozen turbulence hypothesis. This method relies upon turbulent characteristics as input, such as lengthscales, intensity and mean onset velocity. In order to accurately predict loading site specific conditions are needed as input.

Site and System Conditions

Understanding the variation in unsteady loading at a tidal site relies on knowledge of the site conditions. The full-scale tidal site examined here is the EMEC test site in the Fall of Warness, Scotland. Data from this site was acquired as part of the ReDAPT project. Numerous devices were used to monitor the conditions on and around the turbine, as shown in [12]. The focus of this work is to compare conditions at two locations within the tidal site, the chosen locations are shown in Figure 1. The properties of the two ADCPs chosen are given in Table 1 and have also been used in previous studies by [7,12,13].

The positions circled on Figure 1 correspond to the locations of two ADCP at approximately the same depth in the site. The data from these ADCPs have been chosen as they are located at the sides of the turbine, at a distance of approximately 2 turbine diameters. This distance is given in the design standards [8] as a suitable position to define the onset flow the turbine will experience, as they will not experience a large impact from the wake of the turbine. The data obtained from the ReDAPT project gathered velocity measurements for a concurrent period of time. In this study, a period of 70 days is used, which includes 5 tidal cycles for each device location. The spatial variation of onset flow is examined through the turbulence characteristics, vertical shear profiles and the potential influence of waves. In addition to examining the load variation between site location, the variation in turbine depth will also be examined. Figure 2 shows a diagram of the position of the two turbines along the vertical direction. The two turbine positions are chosen to represent the location of a bed-mounted turbine versus a floating turbine. In each case, the same turbine dimensions and blade geometry is used, for comparison, in reality floating turbines are slightly smaller in dimension to those installed as bed-mounted.

Table 1. Device information from the two RDI Workhorses used in the ReDAPT Project [13].

Device	Location A	Location B
Bin Size (m)	1	1
Sample Rate (Hz)	0.5	0.5
Initial Bin Height (m)	3.1	3.1
Latitude (deg)	59.1370	59.1367
Latitude (deg)	−2.805	−2.806

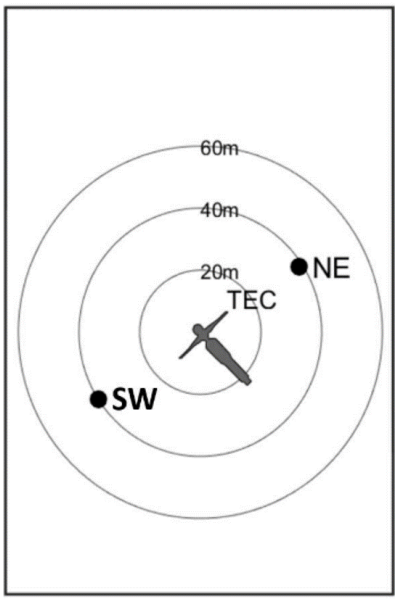

Figure 1. Location of turbine (TEC) and two recording devices used in the ReDAPT project, obtained from [13], data used here from the device at the North East location (NE).

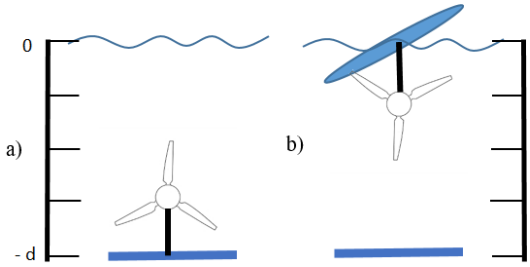

Figure 2. Turbine heights, for (**a**) a bed mounted turbine with hub height (z_{hub}) at approx $-2/3$ depth (d) and (**b**) a floating turbine position with z_{hub} at approx $-1/3$ depth.

For each turbine location and position the operational points are defined using the rotor-disk averages (U_{DA}). This is used, as the rotor average velocity is needed to normalise the power and the thrust coefficient and describes the variation of the velocity that the blade sees as it rotates. However, since only a vertical profile is measured these different disk averages are calculated not using a spatial variation across the whole rotor plane but by using a power weighted average vertical strip wise method, as described in [14]. Here, the measured velocity from the two ADCPs is given at 'z' positions down the rotor plane, at increments dz The disc averages are then calculated using Equation (8):

$$U_{DA} = \left[\frac{1}{A_D} \sum_{i=1}^{n} U_i^3(z) A_i \right]^{1/3}, \tag{8}$$

where A_D is the rotor area, $U_i(z)$ is the velocity at each vertical strip across the disk and A_i is the area of the horizontal strip of height dz, and centreline at z_i, extending across the width of the circular swept area of the rotor calculated as, $A_i = 2(R^2 - (z_i - z_{hub})^2)^{1/2} dz$. For each location and position the range of samples across the 70 day period is shown in Figure 3. Following the design standards [8] the velocities are sampled at 10 min intervals and are binned in 0.2 m/s segments. For location A, there is a larger range of velocities, with location B having a larger number of samples at lower velocities. Based upon these results, one flow speed will be used to compare the load variation between site and position, using detailed measured profiles vs predicted profiles, with the range of samples for each location and position used to inform long term loading.

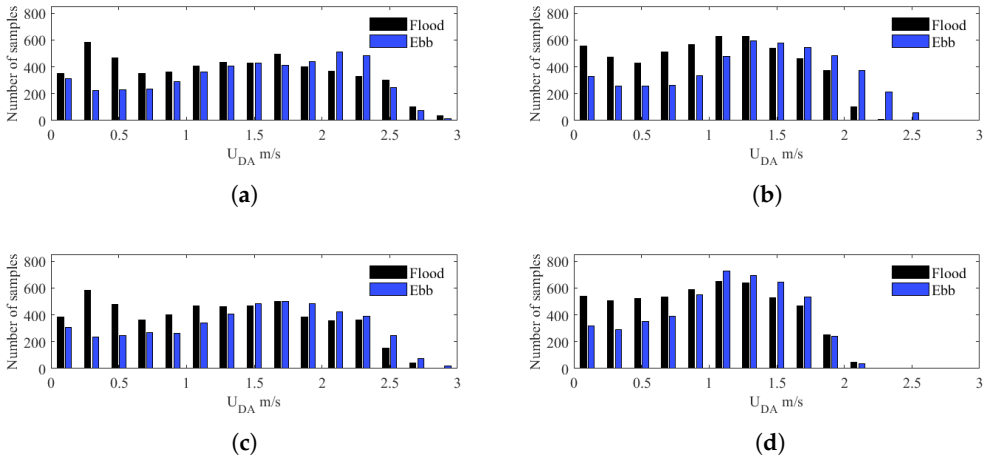

Figure 3. Number of samples for each vertical turbine position at each turbine location in the site, for a range of U_{DA}, between September and November 2014. (**a**) Near Surface, Location A. (**b**) Near Surface, Location B. (**c**) Near Bed, Location A. (**d**) Near Bed, Location B.

2. Flow Field Characterisation

With this work aiming to demonstrate the variation in loading for a turbine located at different positions and depths, using full scale site data, a range of conditions are modelled and the cases examined in this study are shown in Table 2.

Table 2. Set up for different cases in order to examine the variation in load from each case.

Cases	**Shear Profile**		**Turbulence**	
	Varying	Average	Varying	Constant
A	✓		✓	
B	✓			✓
C		✓	✓	
D		✓		✓

In addition to the variation in loads from shear and turbulence, the impact of waves on the loading will be examined using the measured varying profiles and varying turbulence. The operational conditions are defined primarily through the U_{DA} with the calculated power weighted average providing a comparison point between turbine heights and locations. The calculated U_{DA} values are binned, as shown in Figure 3. For each set of binned velocities the characteristics of the onset flow are determined.

2.1. Onset Shear

Using measurements from each ADCP allows a depth variation of velocity at a each location to be measured. This has enabled analysis of the turbines at varying heights with transverse site variation. It allows better understanding of the unsteady loading that the turbine could experience. It is generally understood that at most tidal sites a shear profile is present in the onset flow. A power law profile is commonly used to define the shear profile, work by [15] shows that a 1/7th power law profile can adequately describe the shear. The variation in shear from the measurements is used for each of the onset flows considered, this is compared to a series of predicted profiles. These predicted profiles are calculated based upon a multi-parameter model to predict the variation of shear at the tidal site, for the EMEC test site specifically. These parameters have been defined in [16] who have calibrated the values to the measurements from the ReDAPT project, where MIKE3 was used to model the EMEC test site in the Fall of Warness, UK. This model was validated using current speed and direction, water depth and vertical shear profiles. It was found during this work that although a power law closely followed the vertical variation in the

flood tide it did not capture the more complex flow variation in the ebb tide. Therefore in order to predict the profiles, a quadratic profile was fitted and the coefficients were mapped out in [16]. This approach has been taken here to predict the shear profiles for both the flood and ebb tides. Figure 4 shows the range of shear profiles from the measured ADCP data and the range from the predicted profiles, for a flow speed bin of 1.8–2.0 m/s. For both locations, the flood tide is well predicted using the modelled profiles when compared to the measured variation, with the overall mean being very similar. For the ebb tide, for both locations, the measured profiles spread across a large range, almost parabolic for some cases. At location A the predicted range of profiles for the ebb tide span across a wide range, encompassing the measured range, but that is not replicated at location B, where the predicted range is more refined.

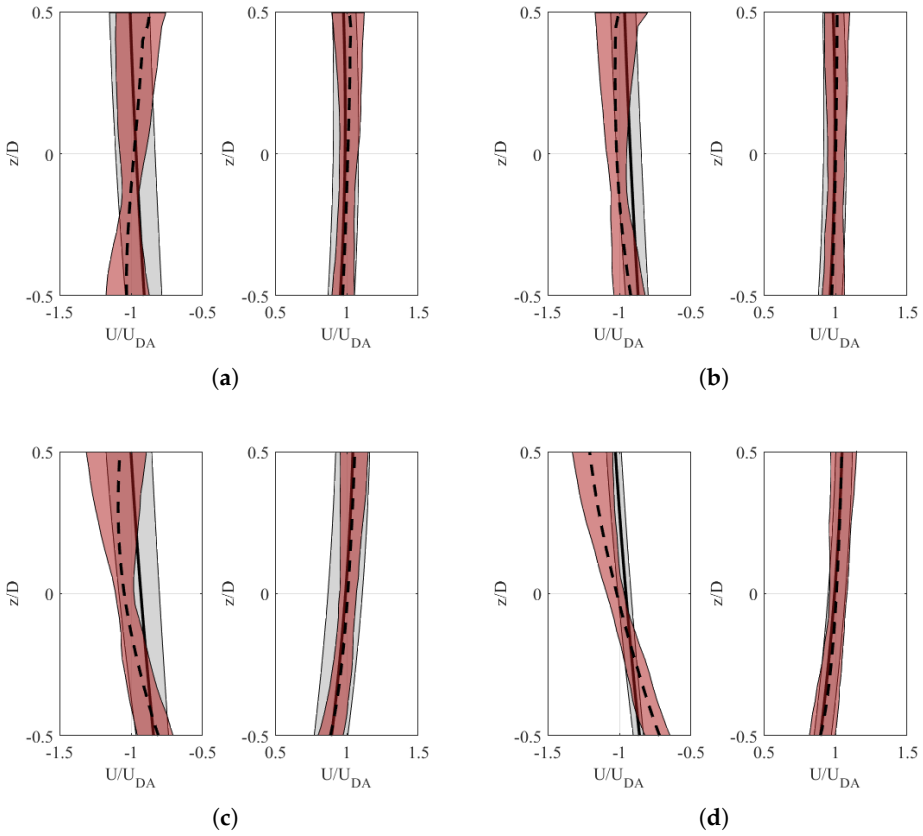

Figure 4. Range of shear profiles for one flow speed case, at two different location and two hub heights, near surface with an origin at $z_{hub} = -15$ m and near bed with an origin at $z_{hub} = -28$ m, for varying measured profiles (red band), varying predicted profiles (grey band), mean measured (dashed black) and mean predicted (solid black). (**a**) Near Surface, Location A. (**b**) Near Surface, Location B. (**c**) Near Bed, Location A. (**d**) Near Bed, Location B.

In order to investigate the influence of waves on loading, the cases which have been shown to represent waves ($H_S > 0.5$ m) are removed from the analysis of the shear profiles. The resultant variation in shear profiles for each location and turbine position is given in Figure 5. In Figure 5 the original variation from all cases is compared to the variation from the reduced cases. For both locations and positions, there is little difference in the range of shear profiles for the flood tide. For the ebb tide, there is also little variation in the range for the near bed turbine, however for the near surface turbine there is a much larger difference, showing a reduced range for the without waves case.

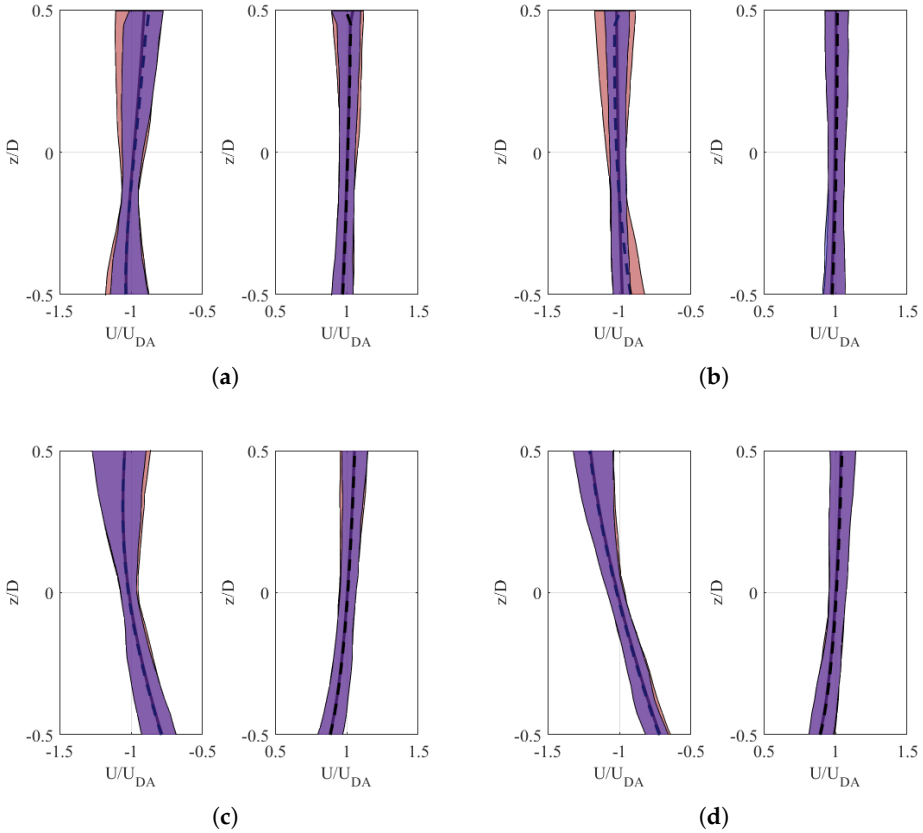

Figure 5. Range of shear profiles for one flow speed case, at two different location and and two hub heights, near surface with an origin at $z_{hub} = -15$ m and near bed with an origin at $z_{hub} = -28$ m, for varying measured profiles (red band), without waves (blue band), mean measured (dashed black) and mean with waves (solid black). (**a**) Near Surface, Location A. (**b**) Near Surface, Location B. (**c**) Near Bed, Location A. (**d**) Near Bed, Location B.

The influence of these shear profiles will be determined by including the variation of velocity onto the frozen turbulence field in order to calculate the impact on the relative velocity and inflow angle to the blade. In addition to the influence of shear, the measured turbulence characteristics are investigated in order to include appropriate parameters into the turbulence field.

2.2. Turbulence Characteristics

Firstly, the turbulence intensity is determined, this value is defined using Equation (9). For each binned velocity values the intensity is determined for all cases. As this could include variations in velocity which are not solely due to turbulence, the intensity values are referred to as fluctuation intensity.

$$I = \frac{u'}{\bar{u}}, \tag{9}$$

where $\bar{u}$ is the mean velocity and u' is the root-mean-square of the velocity fluctuations. The fluctuation intensity is calculated for each location and hub height and shown in Figure 6. These results are consistent with previous published data from the EMEC test site, with a decreasing value of TI with flow speed. At location A, the near surface turbine has greater variation in intensity across the lower velocity bins (0.5–1.5 m/s) compared to the near bed turbine. For location B the near bed turbine shows higher intensity values for U_{DA} greater than 0.9 m/s, as there are a reasonable number of samples used up to a U_{DA} of 2.1 m/s, the difference in intensity values at location B, may be due to changes in bathymetry causing greater bed generated turbulence when compared to location A.

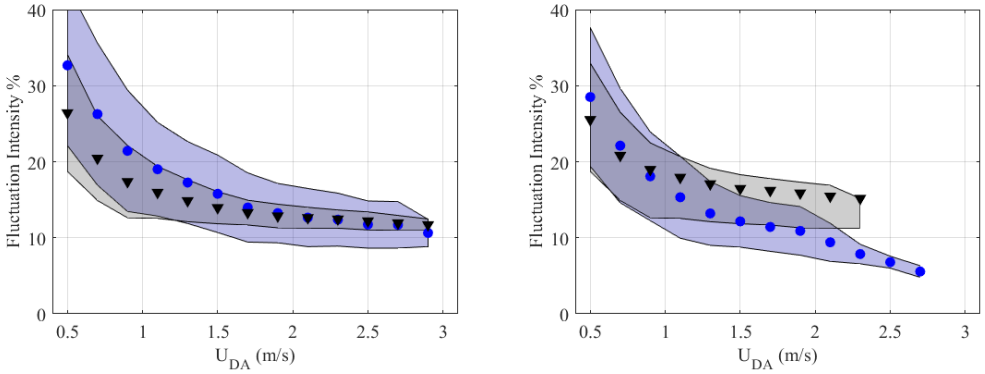

Figure 6. Variation of fluctuation intensity at each hub height and site location, with solid markers showing the mean and shaded region given to show the range around the mean, blue band/blue marker—near surface position, grey band/black marker—near bed position. (**a**) Location A. (**b**) Location B.

Considering the devices are at the same site this shows a definite variation in spatial conditions. The impact of the increased fluctuations on the fatigue loads is investigated. For both locations, the top turbine positions have a larger mean fluctuation when there are a significant number of samples, as expected with the interference caused by waves on the velocity fluctuations near the surface. This influence is investigated by using published wave data, and discarding all samples where the wave height is determined to be greater than 0.5 m. The fluctuation intensity calculated across the cases where waves are not found to be present is shown in Figure 7.

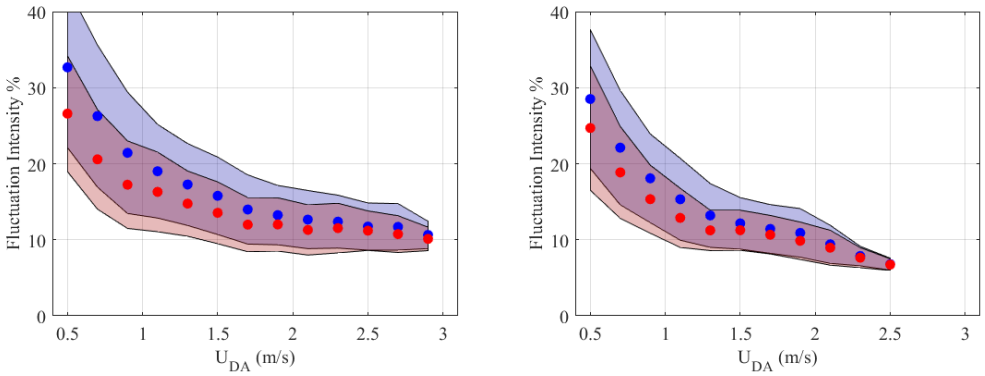

Figure 7. Variation of fluctuation intensity at each near surface hub height for each site location, with solid markers showing the mean and shaded region given to show the range around the mean, blue band/blue markers—all samples, red band markers—without wave cases. (**a**) Location A. (**b**) Location B.

In addition to the value of fluctuation intensity experienced by the turbine, the turbulence lengthscales are calculated in order to simulate the inflow using a frozen turbulence model. The calculation of turbulence lengthscale utilises the 10 min intervals of onset flow data. The lengthscales are calculated for each vertical velocity set using an auto-correlation method. The lengthscales have been determined for the velocity bins, with the results for the 1.8–2.0 m/s velocity bin given in Table 3.

Table 3. Integral lengthscales calculated from measured data for one flow speed case, for all samples and with wave cases removed.

Turbine Position	Integral Lengthscales (m)	
	All Samples	Waves Removed
Near Surface, Location A	13.43	13.06
Near Surface, Location B	14.14	10.79
Near Bed, Location B	14.41	19.39
Near Bed, Location B	11.37	13.22

The flow field is generated using the NREL Turbsim software, with a pre-defined variation of lengthscale and turbulence intensity. For each location and position the turbulent flow field is generated, for the top turbine position a flow field is recreated with a calculated hub height lengthscale within 8% of the calculated values. For the bottom cases integral lengthscales are determined to within 7% of the measured cases. The influence of removing the 'wave' cases causes the average lengthscale to vary, with a 5 m increase for the near bed case at location B, caused by a skew of the remaining non-wave cases.

3. Results

This section will compare the loading generated using the blade element model, initially for one onset flow speed (1.8–2.0 m/s) to determine the influence of the variation in operational conditions. A comparison will be made in this section between the loads calculated using the operational conditions shown in Table 2. Figure 8 shows the normalised damage equivalent loads using case A from Table 2 for both the range of measured and predicted profiles. These loads are normalised by the measured case A at location A for the flood tide. For both locations, the measured and predicted loads with the flood tide are within 5%. For the ebb tide, there is greater variation in loads between location, with the near bed turbine having greater variation between the predicted and measured profiles, consistent with the variation of shear. However the large increase in the loads for the near bed turbine, especially for the ebb tide at location B, is related to the greater magnitude of the fluctuation intensity, compared to the near surface turbine.

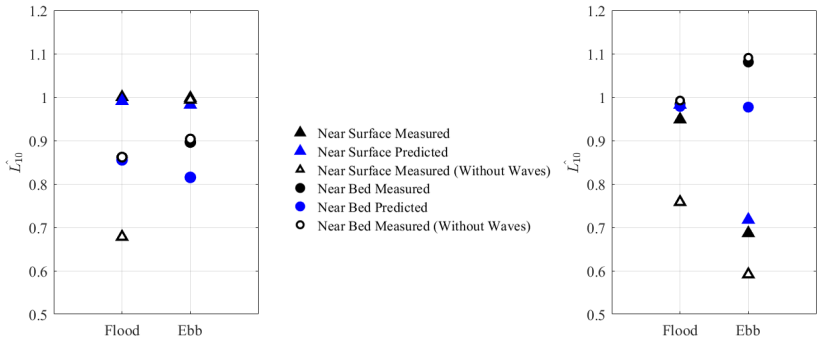

Figure 8. Normalised damage equivalent loads for each turbine position and location, calculated using the measured shear profiles and varying fluctuation intensity, with all samples and with wave cases removed. (**a**) Location A. (**b**) Location B.

Between the two locations, the near surface turbine has loads within 5% during the flood tide; however, for the ebb tide, these loads are as much as 30% different. For the near bed turbine, there is a 15% difference with the flood tide and 30% difference with the ebb tide. A reduced number of cases have been calculated for the measured cases where waves are not considered to be present and are shown in Figure 8. For the near bed case, for both locations, removing the waves has little impact on the DELs calculated. For the near

surface case the flood tide shows a large decrease in the DELs, a 32% decrease at location A and a 19% decrease at location B. This decrease in load highlights the potential influence of waves, especially on a turbine located higher in the water depth. The range of predicted and measured profiles are averaged to give a single defining profile, combined with the average fluctuation intensity for each position and location. The damage equivalent loads for these cases are shown in Figure 9 and compared to the measured varying case from Figure 8. At location A, there is a 20% decrease in DEL for the near surface turbine between the measured average and measured varying cases, for the near bed turbine position the predicted average case is within 4% of the measured varying case with the flood tide and 11% for the ebb tide. At location B, the near bed turbine is lower for the predicted average case compared to the measured varying case for both flood and ebb tide by at least 30%. These loads are determined for a 70 day period in the autumn, with greater variations expected in winter months versus summer, as shown by the variation of wave conditions over a period of a year in [17].

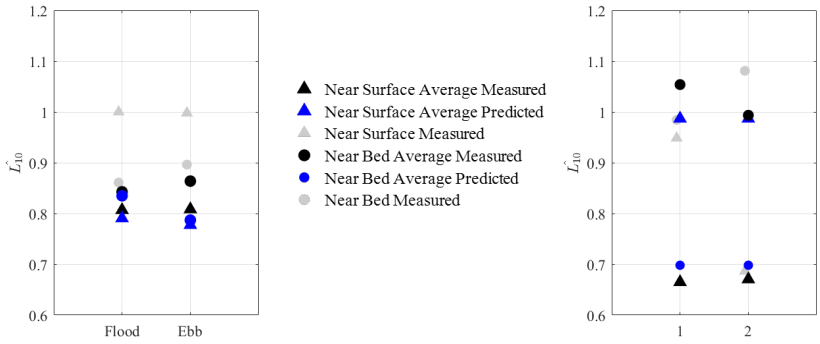

Figure 9. Normalised damage equivalent loads for each turbine position and location, calculated using the measured shear profiles and varying fluctuation intensity, with all samples and with wave cases removed. (**a**) Location A. (**b**) Location B.

Long Term Loading

Long term loading is considered over the full range of U_{DA} values which are given in Figure 3 for a 70 day period. Since this covers multiple tidal cycles and the influence of wave conditions have been removed for some cases, this is assumed to show a reasonable representation of annual loads. For each flow speed, the number of samples is used to determine the total number of load cycles needed to calculate the damage equivalent loads. Using the average predicted profiles and mean fluctuation intensity the damage equivalent loads are calculated for each velocity bin. These are compared to loads from a range of measured varying profiles with varying turbulence intensity and shown in Figure 10. In all cases the value used to normalise the DEL is based upon the maximum load for the 1.8–2.0 m/s flow speed bin for case A. The repetition frequency used to determine the damage equivalent loads is the same for all flow speeds, to allow for comparison. Within Figure 10 the fully measured case (case A) is estimated for comparison to the predicted case (case D) at location A. For the near bed turbine at this location loads determined for each case are within 2%, for the near surface turbine the load variation is greater and increases with flow speed. The range of damage equivalent loads for location B are also given in Figure 10 for the predicted case D. These are greater for the near bed case than the near surface case. These loads are also greater than location A, which is consistent with the variation of fluctuation intensity shown in Figure 6. For three flow speed ranges at location A, a comparison is made between the measured varying cases (case A) for all samples and with waves excluded. For the cases where waves are removed there is a decrease of calculated DEL for the near surface turbine at location A in the flood tide. This decrease is

due to the 2–2.5% decrease in fluctuation intensity found for the flood tide when the wave cases are removed. For the ebb tide, the decrease of fluctuation intensity is less than 0.3%.

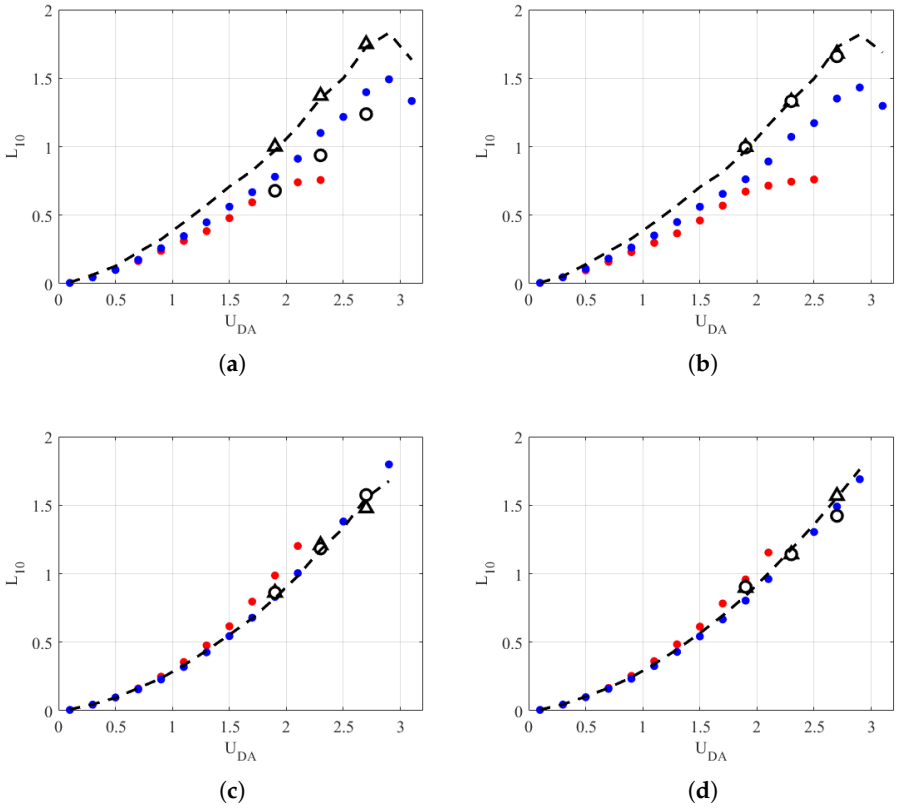

Figure 10. Normalised DEL for the range of flow speeds for each turbine position and tide. Predicted mean profiles and constant turbulence for location A (blue dot), predicted mean profiles and constant turbulence for location B (red dot), measured varying profiles and turbulence (black triangle), measured varying profiles with wave cases removed (black circle) and estimated loads from measured varying profiles (black dash). (**a**) Near Surface, Flood. (**b**) Near Surface, Ebb. (**c**) Near Bed, Flood. (**d**) Near Bed, Ebb.

Using the range of load cycles for the predicted case at each flow speed and at both locations the aggregated DEL is calculated and given in Table 4. These aggregated loads show a 6% variation in loads between the turbine positions at location A, with a 19% variation in loads at location B, with the near bed turbine having higher loading at both locations. Between site locations, there is found to be a 41% difference in load between the near surface turbine position and a 28% difference for the near bed, with location B experiencing lower loading.

Table 4. Normalised damage equivalent load values, using the mean predicted profiles, determined using aggregate load cycles for each flow speed with constant turbulence.

	Location A			Location B		
	Flood	**Ebb**	**Both**	**Flood**	**Ebb**	**Both**
Near Surface	1.04	0.99	1.01	0.57	0.62	0.60
Near Bed	1.09	1.10	1.07	0.80	0.77	0.79

4. Conclusions

Spatial variation of conditions is important to understand as it leads to a variation in DEL. Analysis of the turbulence characteristics shows a similar magnitude and trend between turbine positions at location A, but a different magnitude is found at location B.

This corresponds to larger damage equivalent loads at the near bed turbine at location B when compared to location A. When the average profiles are used to determine the loads at location A, those from the predicted case are found within 4% for the near bed case and are 20% for the near surface. This highlights that the variation in fluctuation intensity found at the near surface influences the calculated damage equivalent loads.

When the influence of waves has been removed the near surface turbine loads are within 6% for the flood tide between each location. With the near bed turbine showing greater variation between location, but less influence between the loads calculated for all samples and those without waves. With the case without waves at location 30% lower then using all samples. Highlighting the need to understand the impact of waves, especially on the loading for turbines located closer to the surface.

When long term loading is considered, the average predicted profiles are used to determine the aggregated loading. For location A, there is a 6% difference between the turbine positions, with the near bed turbine experiencing higher DELs. For location B, there is a 19% difference in DELs, with the near bed also experiencing the higher loads. Between locations, the turbine at location A experiences greater loading, by as much as 40% for the near surface turbine. One of the factors that will impact the aggregated DELs is the range of flow speeds, which is lower for location B. Regardless, the analysis of the two locations and turbine positions highlights the need to understand the unsteady loading conditions at multiple positions within a tidal site.

The model used here is an efficient blade element model, with a frozen turbulence field used as inflow. Further improvements for modelling the unsteady loading can be achieved through the use of a detailed CFD model, such as an actuator line model using an LES inflow.

Author Contributions: Original draft preparation, H.M.; writing—review and editing, H.M. and T.S.; supervision, T.S.; project administration, T.S.; funding acquisition, T.S. Both authors have read and agreed to the published version of the manuscript.

Funding: This research was funded by Interreg TIGER.

Data Availability Statement: Site data was provided by Brian Sellar, University of Edinburgh, from work conducted in the ReDAPT project.

Acknowledgments: This work is supported by the the Tidal Stream Industry Energiser project (TIGER), co-financed by the European Regional Development Fund through the INTERREG France (Channel) England Programme.

Conflicts of Interest: The authors declare no conflict of interest.

References

1. Olczak, A.; Stallard, T.; Feng, T.; Stansby, P.K. Comparison of a RANS blade element model for tidal turbine arrays with laboratory scale measurements of wake velocity and rotor thrust. *J. Fluids Struct.* **2016**, *64*, 87–106. [CrossRef]
2. Apsley, D.D.; Stallard, T.; Stansby, P.K. Actuator-line CFD modelling of tidal-stream turbines in arrays. *J. Ocean. Eng. Mar. Energy* **2018**, *4*, 259–271. [CrossRef]
3. Ahmed, U.; Apsley, D.; Afghan, I.; Stallard, T.; Stansby, P.K. Fluctuating Loads on a Tidal Turbine Due to Velocity Shear and Turbulence: Comparison of CFD with Field Data. *Renew. Energy* **2017**, *112*, 235–246. [CrossRef]
4. Mullings, H.R.; Stallard, T. Assessment of tidal turbine load cycles using synthesised load spectra , including blade-scale fluctuations. In Proceedings of the 13th European Wave and Tidal Energy Conference, Napoli, Italy, 1–6 September 2019; pp. 1–9.
5. McCann, G.N.; Rawlinson-smith, R.I.; Argyriadis, K. *Load Simulation for Tidal Turbines using Wind Turbine Experience*; Technical Report; Garrard and Hassan Ltd.: London, UK, 2007.
6. Milne, I.A.; Sharma, R.N.; Flay, R.G.J.; Bickerton, S. The Role of Onset Turbulence on Tidal Turbine Blade Loads. In Proceedings of the 17th Australasian Fluid Mechanics Conference, Auckland, New Zealand, 5–9 December 2010; pp. 1–8.
7. Parkinson, S.G.; Collier, W.J. Model validation of hydrodynamic loads and performance of a full-scale tidal turbine using Tidal Bladed. *Int. J. Mar. Energy* **2016**, *16*, 279–297. [CrossRef]
8. DNV-GL. Standard Tidal Turbines (DNVGL-ST-0164). 2015. Available online: http://rules.dnv.com/docs/pdf/DNV/ST/2015-10/DNVGL-ST-0164.pdf (accessed on 20 August 2021).
9. Downing, S.D.; Socie, D.F. Simple rainflow counting algorithms. *Int. J. Fatigue* **1982**, *4*, 31–40. [CrossRef]

10. Weller, S.D.; Thies, P.R.; Gordelier, T.; Johanning, L. Reducing Reliability Uncertainties for Marine Renewable Energy. *J. Mar. Sci. Eng.* **2015**, *3*, 1349–1361. [CrossRef]
11. Blackmore, T.; Myers, L.E.; Bahaj, A.S. Effects of turbulence on tidal turbines: Implications to performance, blade loads, and condition monitoring. *Int. J. Mar. Energy* **2016**, *14*, 1–26. [CrossRef]
12. Sellar, B.G.; Wakelam, G.; Sutherland, D.R.; Ingram, D.M.; Venugopal, V. Characterisation of tidal flows at the european marine energy centre in the absence of ocean waves. *Energies* **2018**, *11*, 176. [CrossRef]
13. Sutherland, D.R.J.; Sellar, B.G.; Venugopal, V.; Borthwick, A.G.L. Effects of Spatial Variation and Surface Waves on Tidal Site Characterisation. In Proceedings of the 12th European Wave and Tidal Energy Conference, Cork, Ireland, 27 August–2 September 2017; pp. 1–8.
14. McNaughton, J.; Harper, S.; Sinclair, R.; Sellar, B. Measuring and Modelling the Power Curve of a Commercial-Scale Tidal Turbine. In Proceedings of the 11th European Wave and Tidal Energy Conference, Nantes, France, 6–11 September 2015; Volume 1, pp. 1–9. [CrossRef]
15. Togneri, M.; Masters, I.; Orme, J. Incorporating Turbulent Inflow Conditions in a Blade Element Momentum Model of Tidal Stream Turbines. In Proceedings of the Twenty-First (2011) International Offshore and Polar Engineering Conference, Maui, HI, USA, 19–24 June 2011; Volume 8, pp. 757–762.
16. Gunn, K.; Stock-Williams, C. *Fall of Warness 3D Model Validation Report*; Technical Report; ETI ReDAPT: Loughborough, UK, 2014.
17. Sellar, B.G.; Sutherland, D.R.; Ingram, D.M.; Venugopal, V. Measuring waves and currents at the European marine energy centre tidal energy test site: Campaign specification, measurement methodologies and data exploitation. In Proceedings of the OCEANS 2017—Aberdeen, Aberdeen, UK, 19–22 June 2017; IEEE: Piscataway, NJ, USA, 2017; Volume 2017, pp. 1–7. [CrossRef]